# Interferometric Study of Transition from Weak to Strong Penetration of a Polymer Solution into a Porous Silica Bead

**Iwao Teraoka**

*Department of Chemistry, Polytechnic University, 333 Jay Street, Brooklyn, New York 11201*

*Received August 7, 1995; Revised Manuscript Received January 9, 1996*[⊗]

ABSTRACT: The concentration equilibrium of polymer molecules with a porous medium was studied using a Jamin interferometer and digital image analysis. A porous silica bead was immersed into a solution of the polymer in a solvent isorefractive with silica. The concentration of the polymer in the porous medium was measured as the concentration in the exterior solution was changed in a wide range from dilute to semidilute. For all the chain dimensions studied, the partition coefficient increased to a value close to unity, as the exterior solution became semidilute, a result in agreement with theoretical predictions of the weak-to-strong penetration transition. The transition was, however, found to be more diffuse than predicted. The difference can be partly ascribed to a distribution in the effective pore diameter of the network-structured porous medium.

## Introduction

Exclusion of high molecular weight polymer molecules from porous materials with small cavities underlies gel permeation chromatography (GPC) or size exclusion chromatography.[1] Although there is a constant flow of mobile phase through a column packed with beads of porous materials, GPC is rather understood in terms of partitioning of polymer molecules between the stationary phase (pore channels) and the surrounding mobile phase. Every small volume in the column that encompasses the two phases reaches concentration equilibrium before the mobile phase is transferred to the next plate. The equilibrium is represented by a partition coefficient $K$, defined as the ratio of the polymer concentration in the pore channels to that in the exterior solution.

In the absence of surface adsorption or chain−chain interactions, the partitioning is governed purely by a change $\Delta S$ in the conformational entropy experienced by an isolated polymer chain when it is transferred from the exterior solution into the pore channels. In the dilute solution limit, the partition coefficient $K_0$ is given by[1]

$$K_0 = \exp(\Delta S/k_B) \tag{1}$$

where $k_B$ is the Boltzmann constant. When the radius of gyration $R_g$ of the polymer chain in the dilute solution limit is not too small compared with the radius $R_p$ of a cylindrical pore, $-\Delta S/k_B$ is approximately proportional to $(R_g/R_p)^2$.[2,2−4] Thus $K_0$ drops sharply as $R_g$ becomes larger than $R_p$.

The partition coefficient was calculated many years ago for an isolated molecule of a simple geometry. Casassa and co-workers[2,3] derived an expression of $K_0$ for a Gaussian chain (linear and star-shaped) in a cylindrical, spherical, and slab cavities. Giddings et al.[5] calculated $K_0$ for rigid molecules of a given shape such as rodlike and spherical molecules in rectangular and cylindrical pores. In contrast, attempts are scarce to calculate $K_0$ of an excluded volume chain in any cavity geometries. There is a calculation of $K_0$ for an excluded volume chain in a slit,[6] where the chain was modeled as a Gaussian chain perturbed by the excluded volume. A scaling argument was presented for the partitioning of the chain much larger than the pore size.[4] The results are considered to be correct, but the range of the molecular weight is too high to find a relevance to GPC. To the knowledge of the author, the renormalization theory has not been applied to the problem of confinement of polymer chains by a pore of a well-defined geometry. Computer simulation results are mostly limited to those performed for short chains in a small pore.[7−10] In a separate move, partitioning of linear chains of a finite segment length with a confining geometry has been considered theoretically[11] and in computer simulations.[12,13]

It has been realized that chromatograms in GPC depend on the concentration of the injected solution. When the concentration is too high (higher than ca. $^1/_5$ of the overlap concentration $w^*$ defined as $w^* \equiv (2^{1/2}R_g)^{-3}(M/N_A)$, where $M$ is the molecular weight and $N_A$ is the Avogadro's number), the peak retention time shifts to a longer time and the chromatogram is distorted. This overloading effect has led several researchers to the studies of concentration dependence of $K$.[8,14−19] Most concerns centered on a small deviation of $K$ from $K_0$ in the concentration range below $w^*$ and on obtaining the first concentration coefficient $k_p$ in

$$K = K_0(1 + k_p w + ...) \tag{2}$$

Experimental techniques for the measurement of $K$ include a use of concentration detector such as a UV−visible absorption detector and a differential refractometer to measure the difference in the polymer concentration of the exterior solution between before and after the immersion of the porous materials. Employing this technique, Anderson and Brannon[18] estimated $k_p$ for several water-soluble polymers including proteins equilibrated with controlled pore glasses. Earlier, Satterfield et al.[20] conducted the measurement of the concentration dependence of $K$ for three fractions of polystyrene standard with controlled pore glasses. The two results showed that $K$ approached one as the exterior concentration increased. The concentration range was, however, limited to relatively low concentrations, probably because of experimental difficulties in transferring the solution into the sample cell for the measurement.

Computer simulations that cover a wide range of concentrations have been limited to those performed on

[⊗] Abstract published in *Advance ACS Abstracts,* March 1, 1996.

0024-9297/96/2229-2430$12.00/0 

short chains. For all the combinations of polymer chains and a porous medium studied,[8−10] the partition coefficient increased monotonically as the exterior polymer concentration increased. It is to be noted that, especially for short chains, the partition coefficient became even larger than unity at high volume fractions in the exterior solution.[9,10] This inversion was ascribed to the wall effect in which the polymer chains near the pore wall reduce the packing free energy by aligning parallel to the wall.

The concentration dependence of the partitioning is invariably related to a deviation of thermodynamic properties of a polymer solution (in good solvent) from those of an ideal solution as the solute concentration increases. The deviation is well represented by the concentration dependence of the osmotic pressure $\Pi$. The reduced osmotic pressure $P$ defined by $P \equiv \Pi M/(wN_A k_B T)$, where $T$ is the absolute temperature, begins to increase from unity as $w$ increases. The scaling theory predicts that, in the semidilute regime $w \gg w^*$, $P$ scales as $P \sim x^{5/4}$, where $x \equiv w/w^*$.[21] An approximate functional form of $P(x)$ that applies to a wide range of concentrations from dilute to semidilute was introduced by Ohta and Oono[22] using the renormalization group theory:

$$P(x) = 1 + {}^1/_2 ax \exp\{{}^1/_4[(ax)^{-1} + (1 - (ax)^{-2}) \ln(1 + ax)]\} \quad (3)$$

where $a$ ($\cong 3.49$) is a numerical.[23]

A change in the thermodynamic properties alters the partitioning rule at high concentrations. The high osmotic pressure in the exterior solution drives the polymer molecules into the pore channels at a larger proportion where the osmotic pressure is lower, until the equilibrium of the chemical potential is reached. The equilibration in the chemical potential determines the interior concentration $w_I$ for a given exterior concentration $w_E$:[23]

$$\ln w_I + I(w_I/w^*) - \Delta S/k_B = \ln w_E + I(w_E/w^*) \quad (4)$$

where $I(x) \equiv P(x) - 1 + \int_0^x x'^{-1}[P(x') - 1]\, dx'$. The asymptotes are $I(0) = 0$ and $I(x) \propto x^{5/4}$ for $x \gg 1$. Equation 4 assumes the same reference state for the chemical potentials of polymer chains in the pore and in the exterior solution. It also assumes that the confinement does not change the expression for $P(x)$.

It is to be noted that $\Delta S$ also depends on $w$, because screening of the excluded volume effect contracts polymer chains at high concentrations. The expression for the contraction was derived by Ohta and Oono.[22] Teraoka et al.[23] solved the above equation self-consistently in a wide range of $w_E$ for several values of $R_g/R_p$. They employed, for $\Delta S/k_B$, the expression for a Gaussian chain in a cylindrical pore obtained by Casassa.[2] The concentration dependence of $K$ is shown in Figure 1. As $w_E$ increases, the osmotic pressure rapidly increases exterior to the pore, which drives the polymer chains into narrow pore channels at the expense of the reduced conformational entropy. Eventually $K$ approaches unity at high concentrations for any chain dimensions. The chain contraction was found to play a minor role in increasing $K$ compared with the osmotic pressure effect. Daoud and de Gennes called this phenomenon the "weak-to-strong penetration transition".[4,24]

Also note that the concentration equilibrium is temperature independent, as readily seen in eq 4. The equilibration is determined by the concentration alone as long as the solvent is good (athermal) for the polymer.

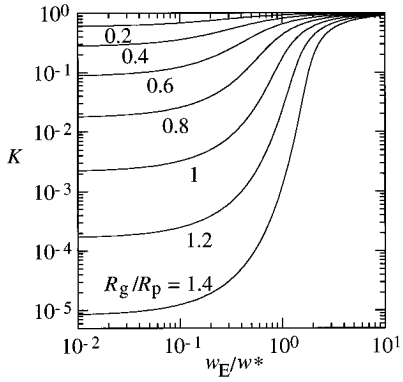


**Figure 1.** Partition coefficient $K$ of a polymer chain with a cylindrical pore of radius $R_p$ plotted as a function of the reduced polymer concentration $w_E/w^*$ in the exterior solution for several values of the ratio of the radius of gyration $R_g$ of the polymer to $R_p$. The ratio is indicated adjacent to each curve.

The weak-to-strong penetration transition was discovered[23] in the course of studying the dynamics of solvated monodisperse polystyrene in the interior of a solid porous glass made of silica with diameter about 1.5 mm. A porous glass bead was equilibrated with the external solution. Index-matching of the solvent with silica made the polymer the only visible species in the three-component system consisting of silica, solvent, and the polymer. Dynamic light scattering was used to obtain the apparent diffusion coefficients $D_I$ and $D_E$ of the polymer in the porous medium and in the exterior solution, respectively. When $w_E \ll w^*$, $D_I$ was identified as that of the center of mass diffusion of polymer molecules hindered by the pore tortuosity. The hindrance was found to be greater for a larger molecular weight polymer. As $w_E$ increases and exceeds $w^*$, $D_I$ rapidly increased. When $w_E > w^*$, $D_I$ depended little on the molecular weight but rather on the monomer concentration, a result indicating that the interior solution was semidilute and the dynamics of polymer molecules were the cooperative diffusion of entangled chains. Furthermore, a large difference between $D_I$ and $D_E$ that existed in the dilute solution regime nearly disappeared at high concentrations, which suggested a nearly equal concentration between the interior and exterior and a correlation length sufficiently smaller than the pore size. The increase in $D_I$ was more striking for a larger molecular weight sample that was expected to have a more dilute interior concentration. The drastic increase in the interior concentration $w_I$ was evident, although $w_I$ was not measured. Teraoka et al.[23] explained the transition as the osmotic pressure-driven migration of polymer molecules into the pore channels.

In this contribution, we report a more direct measurement of the polymer concentration in a porous silica bead in a wide range of polymer concentrations. We take advantage of index-matching between silica and the solvent that renders the situation in which the polymer is the only component that has a refractive index different from the indices of the others. We measure using a Jamin interferometer the optical path for a beam passing through a spherical porous silica equilibrated with a solution of polymer of a given concentration. Digital image analysis of the interference pattern provides information on the polymer concentration in the solution occupying the pore chan-

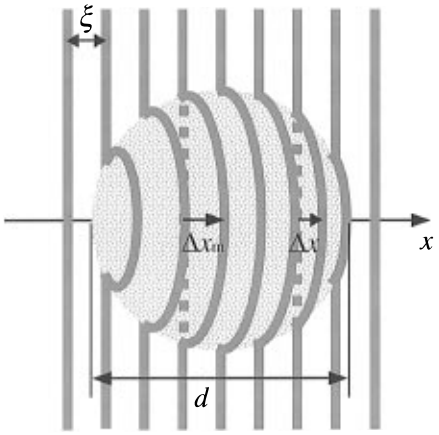


**Figure 2.** Schematic of the interference fringe pattern created by two beams, one of which illuminates a spherical medium suspended in a uniform medium the other beam travels. A slight difference in the refractive index is assumed between the two media. The fringe pattern exterior to the image of the spherical medium is parallel with a period $\xi$. Inside the image of the sphere of diameter $d$, the pattern is displaced. The displacement $\Delta x$ maximizes to $\Delta x_m$ for a fringe at the center of the circular image of the sphere.

nels. We are concerned if the transition from weak to strong penetration is observed in our study when the exterior polymer concentration is increased as theoretically predicted.

Compared with other techniques that measure the difference in the exterior concentration between before and after immersion of porous materials, the interferometry has the following advantages: (1) It is an *in situ* measurement. (2) It requires a small amount of sample solution, typically 1.5 mL. (3) It has a high sensitivity, in particular, at high concentrations. (4) A real time measurement of the interior concentration will enable us to trace the infusion transient of a polymer solution into a solvent-imbibed porous medium and the outflow of the solution from the medium into the pure solvent.

Recently, Thompson and Glandt[25] used integral equations to formulate thermodynamics of linear chains of hard spheres in equilibrium with a porous medium constructed by random, but nonoverlapping deposition of spherical obstacles. They calculated the partition coefficient $K$ as a function of the polymer concentration in the exterior solution. For different chain lengths and porosities, $K$ increased as the concentration increased and approached unity at high volume fractions of the solute. A good agreement was seen between their calculations and experimental results by Satterfield et al.[20]

## Jamin Interferometry

In a Jamin interferometer, two near-parallel laser beams split from a single beam intersect to interfere. Projection of them onto a screen produces an interference pattern of sinusoidally modulated parallel fringes. When one of the beams illuminates a small medium with an average refractive index $n_1$ different from the index $n_2$ of its surrounding the other beam travels, the interference fringe pattern is displaced for the portion of light that has traveled the medium. If the medium is spherical with diameter $d$, the fringe pattern looks like Figure 2. A more detailed account of the pattern is given in the Appendix. Each fringe within a circular rim of the sphere image is an arc of an ellipse that inscribes the circle. A maximum displacement $\Delta x_m$, observed at the center of the circle, and the period $\xi$ of

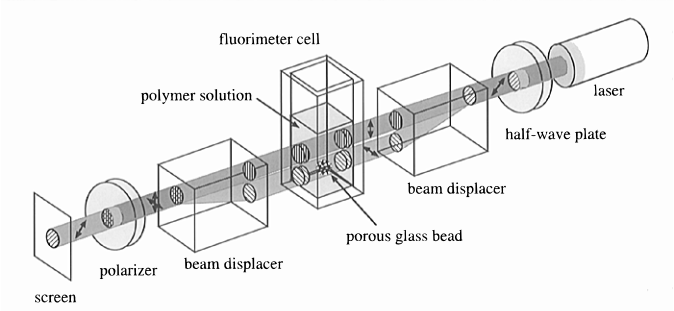


**Figure 3.** Schematic of the Jamin interferometer to measure the polymer concentration in the pore channels of a spherical porous silica in equilibrium with an external polymer solution.

the dark fringes are related to $n_1$ and $n_2$ by

$$\frac{\Delta x_m}{\xi} = \frac{(n_2 - n_1)d}{\lambda} \tag{5}$$

where $\lambda$ is the wavelength of light in vacuum.

In our experiment, the spherical medium is a porous glass bead composed of two phases—a solid phase (mostly silica) and a fluid phase in the pore channels. The length scale of the heterogeneity is about 50 nm, much smaller than the bead diameter ~2 mm. Thus the glass bead can be regarded as a sphere in which the two phases are uniformly distributed. We define the porosity $\rho$ of a porous medium by $\rho \equiv V_{liq}/(V_{liq} + V_{sol})$, where $V_{sol}$ is the solid phase volume and $V_{liq}$ is the volume in the medium filled with the fluid.

The bead is immersed in a polymer solution of concentration $w_E$. The concentration $w_I$ of the solution in the pore channels is generally different from $w_E$. To minimize scattering of light by the glass beads, the solvent used to dissolve the polymer was selected to have a refractive index $n_S$ closely matched to the refractive index $n_G$ of the solid phase of the silica glass. The average refractive index $n_1$ of the porous medium filled with a polymer solution is expressed as $n_1 = (1 - \rho)n_G + \rho[n_S + \Delta n(w_I)]$, where $\Delta n(w)$ is the increment in the refractive index of the polymer solution of concentration $w$ with reference to $n_S$.

The surrounding solution has a refractive index $n_2 = n_S + \Delta n(w_E)$. Therefore from eq 5, $w_E$ and $w_I$ are related to $\Delta x_m/\xi$ by

$$\frac{\Delta x_m}{\xi}\frac{\lambda}{d} = \Delta n(w_E) - \rho\Delta n(w_I) + (1 - \rho)(n_S - n_G) \tag{6}$$

We try to realize the best matching between $n_S$ and $n_G$ by adjusting the temperature, but in general, $n_S - n_G$ is nonzero. The value of the nonzero term $(1 - \rho)(n_S - n_G)$ can be determined from the measurement with the pure solvent $(\Delta x_m/\xi)_0$. Thus we have

$$(\lambda/d)[\Delta x_m/\xi - (\Delta x_m/\xi)_0] = \Delta n(w_E) - \rho\Delta n(w_I) \tag{7}$$

If we obtain in advance the relationship between $\Delta n(w)$ and $w$ using a differential refractometer, the measurement of $\Delta x_m/\xi$ will give us the estimate of $w_I$ for given $w_E$, $\rho$, and $n_S - n_G$.

## Experimental Section

**Interferometer.** Figure 3 is a schematic of the Jamin interferometer constructed for the current study. The polarization direction of a linearly polarized beam from a He−Ne laser (Melles Griot, 5 mW, 632.8 nm) can be changed by rotating a half-wave plate. The beam is then expanded to a nearly collimated circular beam of diameter about 3 mm by a

**Table 1. Characterization of the Polymer Samples**

| sample | $M_p$ | $M_w/M_n$ | $R_g$ (nm) | $w^*$ (g/L) |
|---|---|---|---|---|
| PS30 | $3.03 \times 10^4$ | 1.02 | 5.80 | 91.2 |
| PS49 | $4.90 \times 10^4$ | 1.05 | 7.71 | 62.7 |
| PS89 | $8.93 \times 10^4$ | 1.04 | 11.1 | 38.3 |
| PS164 | $1.64 \times 10^5$ | 1.06 | 15.8 | 24.0 |
| PS289 | $2.89 \times 10^5$ | 1.05 | 22.2 | 15.7 |
| PS402 | $4.02 \times 10^5$ | 1.06 | 26.9 | 12.1 |

set of concave and convex lenses. A beam displacer (Melles Griot) made of a calcite single crystal of length 38 mm splits the beam into two parallel beams separated by 4.0 mm almost vertically. The top and bottom beams, polarized vertically and horizontally, enter a fluorimeter cell (UVONIC type 23; 10 mm × 10 mm base). Inside the cell, a porous glass bead is mounted on top of a Teflon tubing plugged into a fixed stainless steel rod. A polymer solution fills the cell to the level at least 7 mm higher than the top of the glass bead. The bottom beam illuminates the glass bead. The top beam passes through the external solution in equilibrium with the bead. Exiting the cell, the two beams are coupled by another beam displacer of the same length. A polarizer is placed to produce a parallel interference pattern with the best contrast. The pattern is magnified by two convex lenses and projected onto a translucent screen. The lens closer to the cell is mounted on a translation stage to focus the bead image. The fringe pattern on the screen is observed clearly in a domain shared by two round, off-centered bright spots, representing the two beams separated by the first displacer. The center-to-center distance of the spots can be changed by rotating the second beam displacer. The rotation simultaneously changes the period of the fringes. The period maximizes when the two spots coincide. The orientation of the first beam displacer is responsible for the orientation of the fringe pattern. The interferometer is in principle similar to the micro Mach−Zehnder interferometer used by Sernetz et al.[26,27] to measure the porosity and the partition coefficient of water-soluble polymers for a spherical porous gel (cross-linked polymer).

The image of the fringe pattern on the projection screen is captured from the back side of the screen by a Hi-8 video camcorder (Sony CCD-FX710). A video frame is digitized by a built-in frame grabber in a Centris 660AV (Apple Computer). A public domain image analysis program "Image 1.52" (developed at the U.S. National Institutes of Health and available on the Internet by anonymous FTP from zippy.nimh.nih.gov) analyzes the digitized image to yield a period of the dark fringes and their displacement relative to the background pattern.

The fluorimeter cell is held in a cuvette holder (Milton Roy) with a water channel running through it. The temperature of the cell is maintained at 42.0 ± 0.05 °C by water circulating from a refrigerating bath. The cuvette holder is mounted on two translation stages to position the glass bead at the optimal position with respect to the two beams.

**Measurement of the Refractive Index Increment.** Measurements of the difference $\Delta n$ in the refractive index of a polymer solution from that of the pure solvent and $\Delta n$ of a mixture of two solvents relative to one of the solvents were carried out using the differential refractometer KMX 16 (Chromatix; calibrated with NaCl aqueous solutions) at wavelength $\lambda = 632.8$ nm and 42.0 °C.

**Samples.** Polystyrene (PS) samples were purchased from Pressure Chemical. Peak molecular weight $M_p$, the polydispersity index $M_w/M_n$, where $M_n$ and $M_w$ are the number- and weight-average molecular weights, and the radius of gyration $R_g$ are listed in Table 1. The molecular weight data were supplied by the manufacturer. For $R_g$, we used the relation $R_g/\text{nm} = 0.0125 \times M_w^{0.595}$ obtained for a fully swollen polystyrene[28] (a small upward deviation for $M_w < 10^5$ was taken into account). Reagent grade solvents 2-fluorotoluene (2FT) and HPLC grade toluene were purchased from Aldrich and used as received.

Porous glass beads (S980G2.2) were kindly supplied by Shell Development Co. They are nearly spherical and have a diameter of about 2.2 mm. The beads were manufactured in spinodal decomposition followed by acid leaching. The solid phase made of silica and the empty space form a bicontinuous structure. The manufacturer-supplied data show that the average pore diameter is ca. 50 nm and the pore volume is 1.0 $cm^3/g$. The glass beads were surface-treated using chlorotrimethylsilane following the procedure described elsewhere.[29] This procedure is known to produce inert pore walls and prevent adsorption of polystyrene. The concentration of the polymer does not decrease upon immersion of treated glass beads.[30] Diffusion of the polymer inside the glass bead, as studied by dynamic light scattering, is not anomalous, ruling out the presence of polymer chains adsorbed onto the pore walls.[29]

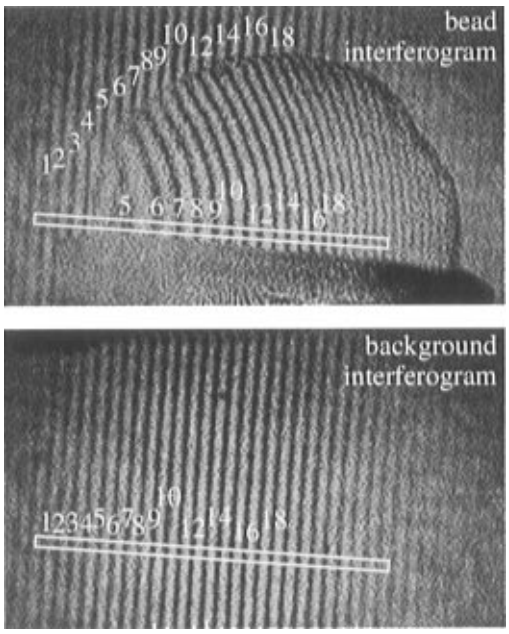


**Figure 4.** Bead interferogram for a spherical porous glass of diameter about 2.2 mm and a corresponding background interferogram. The numbers are indices of the dark fringes. The white-outlined lines at the same location in the two interferograms were used for the profile plotting.

For each of the six PS fractions, a fluorimeter cell with a single porous glass bead was used throughout the concentration equilibrium experiment. The total pore volume is estimated to be 6 $\mu$L, sufficiently small compared with the volume of the exterior solution (~1.5 mL).

## Results

**Measurement of Displacement of the Fringe Pattern.** For each measurement of $\Delta x/\xi$, we first positioned the image of the glass bead at around the center of the two bright spots on the screen and captured a video frame for the bead interferogram. Then we nudged down the cell holder so that the two laser beams travel the external solution above the glass bead and captured another video frame for a background interferogram. All the other optical arrangements including the focus of the camcorder were held unchanged between the two successive captures of the interferogram. Therefore, the fringe pattern exterior to the bead image in the bead interferogram replicates the background interferogram. The orientations of the two beam displacers were adjusted so that the exterior fringe pattern was approximately perpendicular to the upper edge of the image of the supporting tubing and the bead image contained a sufficient number of dark fringes, typically between 25 and 35. An example of a pair of the captured video frames is shown in Figure 4 (part of the 640 × 480 pixel image). The fringes inside the bead image are nearly elliptic, but do not follow an ideal

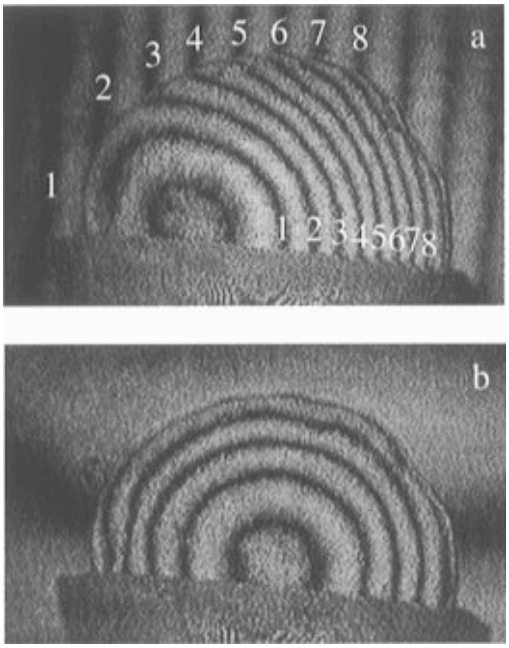


**Figure 5.** Bead interferograms for a large period of fringe pattern. (a) $d/\xi \cong 8.6$; (b) $d/\xi \cong 2.0$. The numbers are indices of the dark fringes.

pattern expected. Asphericality and nonuniform porosity of the glass bead as well as nonuniform refractive index of its solid phase are considered to cause the distortion. In addition, the fringe pattern is subject to imperfections of optical components used in the Jamin interferometer.

The displacement $\Delta x$ of a dark fringe in the bead image is measured with respect to a hypothetical fringe that, in the absence of the bead, would have run straight from the corresponding exterior fringe. To measure the maximum displacement $\Delta x_m$, we indexed the exterior and interior fringes, as shown in Figure 4. The quantity necessary to determine the interior polymer concentration is $\Delta x_m/\xi$. It is independent of $\xi$. Therefore, $\Delta x_m$ increases as $\xi$ increases when the orientation of the beam displacer changes. The example of the bead interferogram is shown in Figure 5a (captured for the glass bead−polymer solution system used for Figure 4; so is Figure 5b explained below). In addition to elliptic arcs, the fringe pattern has two closed dark ellipses (unless blocked by the supporting tubing). Those closed ellipses have the same indices as those of dark fringes running outside of the bead image.

A further increase in $\xi$ is possible by adjusting the distance between the concave and convex lenses in the beam expander. When $\xi$ is comparable to the diameter of the bead image (Figure 5b), nearly all the dark fringes in the bead images are on closed ellipses. The number of those ellipses gives an estimate of the lower and upper bounds for $|\Delta x_m/\xi|$, as shown in the Appendix. This example has four closed ellipses, and $d/\xi = 2.0$, which gives $4.9 < |\Delta x_m/\xi| < 5.9$.

To estimate $\Delta x_m/\xi$, a straight line segment of a finite width (typically 10 pixels) was drawn on the bead interferogram so that it is perpendicular to the exterior fringes and runs along a diameter of the bead image, as indicated by a white outline in Figure 4. The profile plotting in the application *Image* produces the intensity profile as a function of the number of pixels along the line segment counted from the left end. The plot resembles a modulated sinusoidal curve. The intensity profile of the background fringe pattern was obtained

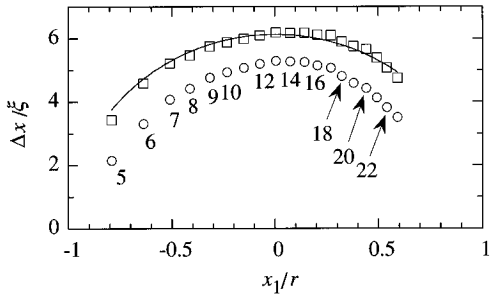


**Figure 6.** Displacement $\Delta x$ divided by the fringe period $\xi$ plotted in circles as a function of $x_1/r$, where $x_1$ is the distance of the fringe from the center of the bead image measured along the equator and $r$ is the radius of the bead image. The numbers are fringe indices. The difference in $\Delta x/\xi$ between a polymer solution and the pure solvent is shown in squares. The solid line is the best fit by an elliptic arc that peaks at $x_1 = 0$ and disappears at $x_1 = \pm r$.

by drawing a line segment at the same location and orientation in the window. The line segment in the bead interferogram included several dark exterior fringes to establish a correspondence between the pixel numbers of the two profile plots and make necessary corrections (typically about 1 pixel) to the estimate of $\Delta x$.

The displacement $\Delta x$ was calculated in terms of pixels as a peak-to-peak distance for each of the indexed dark fringes inside the bead image. The period $\xi$ was calculated as the average of the periods of the dark fringes in the background interferogram that encompass a distance at least the radius of the bead image. Circles in Figure 6 are a plot of $\Delta x/\xi$ for the fringes of indices from 5 to 23, as a function of $x_1/r$, where $x_1$ is the position of the peak intensity relative to the center of the bead, and $r = d/2$ is the radius of the bead image. Appendix shows that $\Delta x$ should maximize for the fringe that passes through the center of the bead image. In most images, $\Delta x$ maximized around the center, but there were beads that had the largest $\Delta x$ at slightly off-centered locations. Furthermore, $\Delta x/\xi$ should change as $(1 - (x_1/r)^2)^{1/2}$, but a deviation from that rule is evident in the plot. The deviation is ascribed to imperfect spherical shape and heterogeneity in the porosity and refractive index of the solid phase of the porous glass bead.

The deviation can be mostly removed by taking the difference in $\Delta x/\xi$ between the measurement at a given polymer concentration and the one at the zero concentration, $(\Delta x/\xi)_0$. Note that $(\Delta x/\xi)_0$ is also a function of $x_1/r$. Squares in Figure 6 are a plot of $\Delta x/\xi - (\Delta x/\xi)_0$. The solid line is the best fit by an elliptic arc that peaks at $x_1/r = 0$ and disappears at $x_1/r = \pm 1$. The fit is reasonable. For all the measurements of the maximum displacement $\Delta x_m/\xi$, simply the value of $\Delta x/\xi$ at $x_1 = 0$ was used.

**Measurement of Porosity.** We first measured a refractive index increment $\Delta n$ of a mixture of 2FT and toluene at 42.0 °C with reference to pure 2FT for five mixture ratios. The weight fraction $\phi_{tol}$ of toluene in the mixture was in the range of $0 \le \phi_{tol} \le 0.2$. The relationship between $\Delta n$ and $\phi_{tol}$ is well described by

$$\Delta n/\phi_{tol} = 2.423 \times 10^{-2} \tag{8}$$

with the average deviation of 0.64%.

The porosity was measured for each surface-treated glass bead (E, F, G, H, I, and J) using mixtures of 2FT and toluene in the range of $\phi_{tol} \le 0.15$. The mixture is considered to fill the pore channels with the same mixture ratio. Then the right-hand side of eq 6 is

**Table 2. Characterization of the Silica Spheres**

| bead | diameter $d$ (mm) | porosity $\rho$ | for PS fraction |
|---|---|---|---|
| E | 2.26 | 0.671 | PS289 |
| F | 2.20 | 0.642 | PS164 |
| G | 2.15 | 0.587 | PS30 |
| H | 2.24 | 0.613 | PS89 |
| I | 2.16 | 0.622 | PS49 |
| J | 2.20 | 0.539 | PS402 |

rewritten as $n_2 - n_1 = (1 - \rho)[n_S - n_G + \Delta n(\phi_{tol})]$. Since $\Delta n \propto \phi_{tol}$, $n_2 - n_1$ depends linearly on $\phi_{tol}$. Comparison of the two linear coefficients gives the porosity $\rho$ as

$$\rho = 1 - \frac{d(n_2 - n_1)/d\phi_{tol}}{d\Delta n/d\phi_{tol}} \tag{9}$$

We first introduced about 1.5 g of pure 2FT into each cell with a glass bead in it. After about 24 h, the interferogram was recorded and analyzed to obtain $(\Delta x_m/\xi)_0(\lambda/d) = (1 - \rho)(n_S - n_G)$. Because of variations in the refractive index among different beads, $(\Delta x_m/\xi)_0$ was different from bead to bead. Then a small amount of toluene (~40 mg) was added into the cell. The tightly capped cell was enclosed in a tightly capped polymer bottle. The bottle was placed on an orbital rotating stage (100 rpm) for at least 24 h to ensure uniform mixture composition throughout the accessible volume. The interferogram was again recorded and analyzed. The addition of toluene and the recording of the interferogram were repeated. At each concentration, two to three pairs of interferogram, different slightly in the period and the orientation in the fringe pattern, were photographed. We thus measured $\Delta x_m/\xi$ at four or five concentrations of toluene. Fitting of the data by straight lines gives the estimates of $\rho$ as listed in Table 2. The value of $\rho$ estimated from the data supplied by the manufacturer of the beads is 0.69. Projection of a bead in the cell rotated by 90° gave an estimate of the diameter $d$.

When the last measurement was completed, the cell was washed several times with pure 2FT, each separated by a day, to be used subsequently for the measurement of the polymer concentration in the interior of the porous medium equilibrated with a PS solution.

**Measurement of Differential Refractive Index.** The differential refractive index $\Delta n$ of a PS solution with reference to the solvent 2FT was measured for two PS fractions, PS49 and PS164. The concentration range was $\phi_{PS} \leq 0.08$, where $\phi_{PS}$ is the weight fraction of PS in the solution. The results are shown in Figure 7. For both PS fractions, $\Delta n$ follows a common straight line given by

$$\Delta n/\phi_{PS} = 0.1340 \tag{10}$$

with the average deviation of 0.03%.

**Measurement of the Partition Coefficient.** Similarly to the porosity measurements, we began with the measurement of $(\Delta x_m/\xi)_0$ using a cell filled with a pure 2FT. The value of $(\Delta x_m/\xi)_0$ was close to that obtained in the measurement of the porosity for each of the six glass beads. Then, we added a PS fraction to the cell. The combination of the glass bead and the PS fraction is listed in Table 2. Unlike low molar mass diffusants such as 2FT and toluene, slow diffusion of the polymer molecules in the porous medium can require a longer equilibration time, especially at high concentrations.[31,32] We verified that $\Delta x_m/\xi$ changed no more than 0.1 between two measurements performed at least 2 days apart. Then, the PS fraction was added again for the measurement at the next concentration. At low concentrations, the equilibration time was typically 3−5 days. At the highest concentrations in our measurements, the time was 30−50 days. The whole measurement that covers from a pure solvent to semidilute solutions required $^1/_2$ to $1^1/_2$ years.

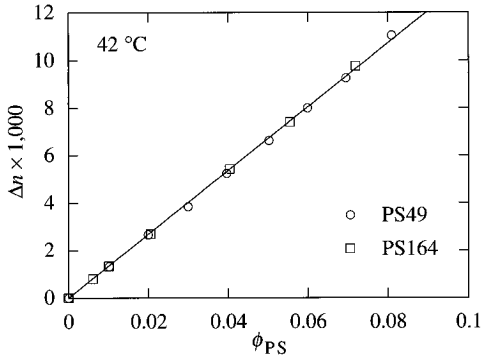


**Figure 7.** Increment $\Delta n$ of the refractive index of a polystyrene solution in 2-fluorotoluene from that of the pure solvent at 632.8 nm, 42.0 °C, plotted as a function of the weight fraction $\phi_{PS}$ of polystyrene. Two different fractions of polystyrene, PS49 and PS164, were used. The line is a best fit of the plots to a straight line that passes through the origin.

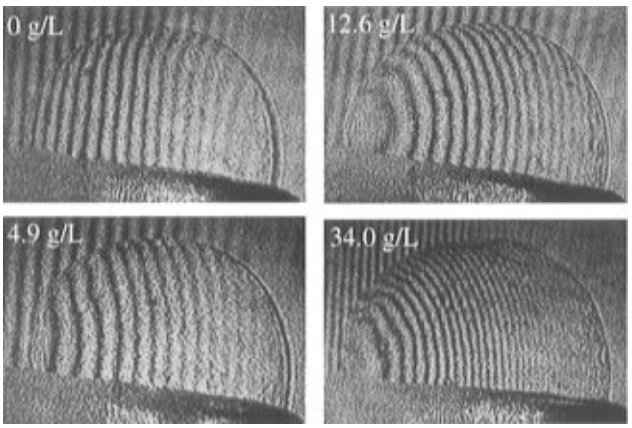


**Figure 8.** Examples of bead interferogram shown for four different concentrations of polystyrene PS402 in the exterior solution.

Examples of the interferogram are shown in Figure 8 at concentrations $w_E = 0$, 4.9, 12.6, and 34.0 g/L for PS402. At $w_E = 0$, the interference pattern penetrates the image of the glass bead nearly unperturbed. As $w_E$ increases, the fringe pattern in the bead image becomes more curved, and the indexing becomes more difficult. There are, however, a couple of clues that help evaluate $\Delta x_m/\xi$ up to about 14:

(1) Try to find a single dark fringe in the bead image that traces clearly through the edge of the glass bead image.

(2) If there are no closed ellipses inside the bead image, the first elliptic arc corresponds to the first exterior fringe that intersects with the bead image. The closed circles correspond to the exterior fringes that do not intersect.

(3) By making the period as large as the bead image, nearly all the elliptic fringes in the bead image will be closed. The Appendix shows how the lower and upper bounds for $|\Delta x_m/\xi|$ are estimated from the number of these ellipses.

Figure 9 shows $\Delta x_m/\xi$ as a function of $w_E$ for PS402. As $w_E$ increased, $\Delta x_m/\xi$ increased, but the slope de-

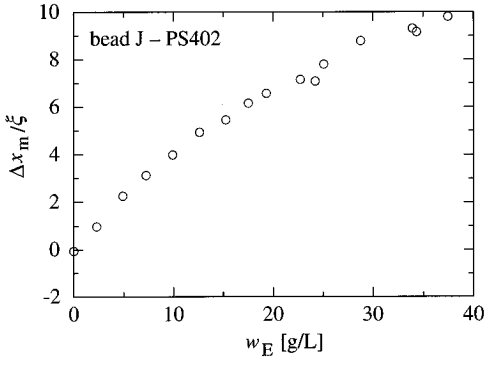


**Figure 9.** Maximum displacement $\Delta x_m$ of a fringe pattern inside the bead image, relative to the fringe period $\xi$, plotted as a function of the polymer concentration $w_E$ in the exterior solution. This example is for PS402 with bead J.

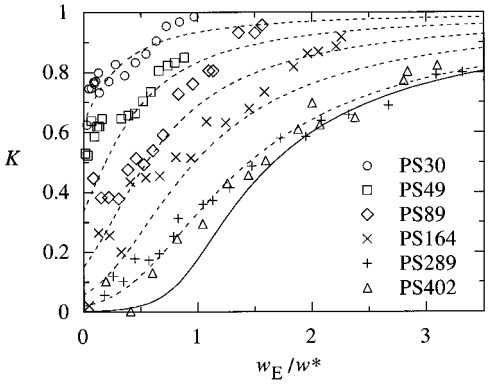


**Figure 10.** Partition coefficients $K$ plotted as a function of reduced concentration, $w_E/w^*$, in the exterior solution for six fractions of polystyrene. Dashed lines represent $K$ calculated for $R_g/R_p = 0.2$, 0.4, 0.6, 0.8, and 1 in a porous medium with a pore size distribution. The solid line is for $R_g/R_p = 1$ in the absence of the distribution.

**Table 3. Partitioning at Low Concentrations**

| sample | $R_g/R_p$ | $K_0$ | $K_0k_p$ (L/g) |
|---|---|---|---|
| PS30 | 0.232 | 0.719 | 0.00294 |
| PS49 | 0.308 | 0.565 | 0.00427 |
| PS89 | 0.444 | 0.308 | 0.0115 |
| PS164 | 0.632 | 0.140 | 0.0184 |
| PS289 | 0.888 | 0.0056 | 0.0210 |
| PS402 | 1.076 | −0.013 | 0.0243 |

creased, implying that the polymer is partitioned in the porous medium at a higher proportion.

Using eqs 6 and 10, we can convert the data points in Figure 9 to those of $K$, the partition coefficient. They are shown in Figure 10 together with $K$ for the other PS fractions. The data points contain large errors when the polymer solutions are dilute, because the estimation of $w_I$ depends crucially on a small difference in $\Delta x_m/\xi$ between the two measurements at $w_E$ and for the pure 2FT.

## Discussion

**Dilute Solution Limit.** The zero concentration asymptote of the partition coefficient, $K_0$, estimated from Figure 10, is listed in Table 3 for the six PS fractions. The negative $K_0$ value for PS402 is due to experimental errors. Symbols in Figure 11 show $K_0$ as a function of $R_g/R_p$. For reference, the formula obtained by Casassa[2] for a Gaussian chain of $R_g$ in a cylindrical pore of radius $R_p$ is shown by a solid line. The asymptotes are located above the line, indicating a larger partitioning to the interior solution than calculated for the Gaussian chain.

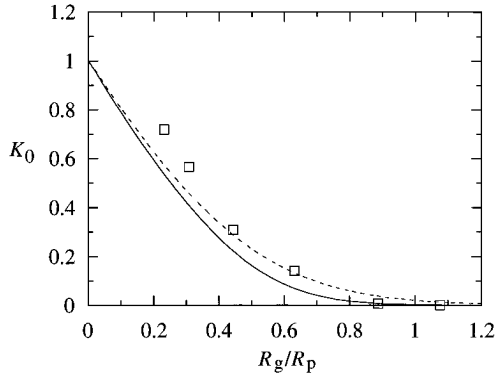


**Figure 11.** Partition coefficient in the dilute solution limit, $K_0$, plotted as a function of $R_g/R_p$. The solid line represents Casassa's result calculated for a Gaussian chain with a cylindrical pore, and the dashed line is with cylindrical pores with a pore size distribution.

This observation is in agreement with experimental data reported by Satterfield et al.[20] and with the computer simulation results by Bleha et al.[8]

If a small fraction of polymer molecules are adsorbed onto the pore walls, it may explain the upward deviation. A more plausible ground will be, however, in the network structure of the porous materials used. Over a short distance, the pore resembles a cylindrical cavity. At the junctions of these cylinders, the polymer chain enjoys a much greater freedom for its conformation. In terms of the effective pore radius of a long cylindrical cavity that provides the same degree of confinement, the network-structured porous medium has a broad distribution in the pore radius, especially at radii larger than the nominal radius. This distribution is considered to have caused the upward deviation of the extrapolated $K_0$. There are no theoretical results or formulations available for the partitioning of a polymer chain with a porous medium fabricated by eching of a bicontinuous medium created in spinodal decomposition. For reference we calculated the partition coefficient for a Gaussian chain with cylindrical pores in which the pore radius follows a normal distribution. The standard deviation was assumed to be 0.3 of the nominal pore radius. The result is shown by a dashed line in Figure 11. The pore size distribution lifts $K_0$, especially when $K_0$ is small, thereby improving agreement with the measured data.

**First Concentration Coefficient.** The first concentration coefficient $K_0k_p$ of the partition coefficient defined in eq 2 was obtained by fitting the data points in Figure 10 by a straight line for each of the six PS fractions in the range where a linear fitting appeared reasonable, and is listed in Table 3. Squares in Figure 12 show the coefficient in the reduced form, $K_0k_p/(2A_2M)$, as a function of $K_0$, where the second virial coefficient $A_2$ was calculated from $A_2 = (1.03 \times 10^{-2})M^{-0.254}$ cm$^3$/g$^2$.[33] The coefficients for PS289 and PS402 have large error bars (not shown). The linear range can be quite narrow for the polymer chains that have a small $K_0$. Also shown are the reduced first concentration coefficients for linear chains in equilibrium with a cylindrical pore of uniform radius (solid line), calculated from the plots in Figure 1, and with cylindrical pores that have the pore size distribution considered above (dashed line). Another theoretical estimate of $K_0k_p/(2A_2M)$ calculated by Thompson and Glandt[25] for four different chain lengths is shown by crosses. Compared with the theoretical curves, the reduced first concentration coefficient exhibits a much weaker dependence on $K_0$. Although the distribution in the pore size brings down

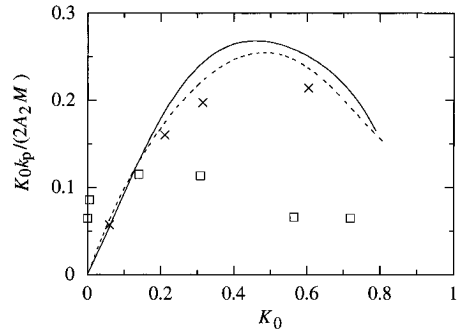


**Figure 12.** First concentration coefficient in the reduced form, $K_0k_p/(2A_2M)$, plotted as a function of $K_0$. The solid line represents the coefficient for linear chains in the cylindrical pore calculated for the results given in Figure 1. With a pore size distribution, the curve is lifted to a dashed line. Crosses were calculated from Thompson and Glandt.

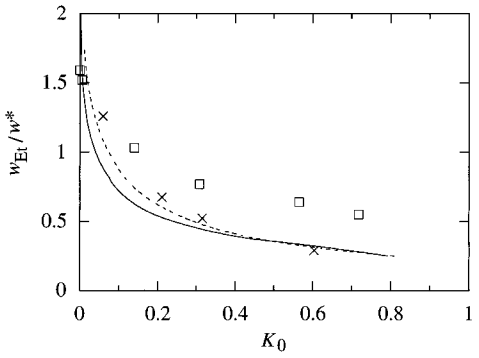


**Figure 13.** Transition concentration $w_t$ plotted as a function $K_0$. The solid and dashed lines represent the concentrations calculated for linear chains with a cylindrical pore of a uniform radius and distributed radii, respectively. See text for definitions. Crosses were calculated from Thompson and Glandt.

$K_0k_p/(2A_2M)$, the distribution alone does not explain the small values.

**Weak-to-Strong Penetration Transition.** For all the PS fractions studied, the partition coefficient $K$ increased, from the value $K_0$ that depends strongly on the molecular weight to a value close to unity. Unlike some simulation results,[9,10] $K$ did not exceed unity. The transition from weak-to-strong penetration took place at a high reduced concentration for a fraction of a larger molecular weight, in agreement with theoretical prediction.[23] The transition was, however, diffuse. We define here a transition concentration $w_{Et}$ as the concentration at which $K$ exceeds the arithmetic average of the low- and high-concentration asymptotes, i.e., $K(w_{Et}) = (1 + K_0)/2$. Those $w_{Et}$ estimated from Figure 10 are plotted in squares as a function of $K_0$ in Figure 13, along with the theoretical curve (solid line) obtained from Figure 1. Except for PS289 and PS402, $w_{Et}$ is systematically higher than that predicted. The transition needed a much higher concentration in the exterior solution. A similar trend was observed in the study of the diffusion coefficient of polystyrene in the porous medium.[23] In the following, we examine some possible causes.

(1) If the osmotic pressure of a polymer solution is lower than that given by the interpolation formula, eq 3, in the concentration range around $w^*$, then the increase in $K$ will be suppressed. The formula was, however, shown to fit well the experimental data obtained by Noda et al.[34] for poly(α-methylstyrene) fractions of $M = 7.08 \times 10^4$ to $7.47 \times 10^6$ in the concentration range of $0.1 \lesssim w/w^* \lesssim 10$. It is therefore difficult to ascribe the smaller $w_{Et}$ to an error in the estimate of the osmotic pressure, at least for fractions with $M > 7 \times 10^4$.

(2) If the polymer chain of a finite length does not contract in the semidilute regime as much as that calculated for a sufficiently long chain, then it will increase $w_{Et}$. To find the effect of the absence of the chain contraction on the weak-to-strong penetration transition, we carried out the self-consistent calculation of eq 4 with chain contraction supressed. The result was a few percent increase in $w_{Et}$. This effect is too small to explain observed large values of $w_{Et}$.

(3) The distribution in the effective pore radius can diffuse the weak-to-strong penetration transition, as $w_{Et}$ spreads over a certain range. The distribution may originate in the network structure of the porous glass beads used, as discussed earlier. The dashed line in Figure 13 shows $w_{Et}/w^*$ calculated for a porous medium with the pore size distribution (normal distribution; standard deviation is 30% of the nominal pore radius). The distribution increases $w_{Et}$ for fractions with $K_0 <$ 0.3. The observed diffuse transition can be partly explained by the distribution. To fully explain the difference, the pore size needs a distribution broader than the one used in the above calculation. The crosses in Figure 13 were calculated from the plot in Thompson and Glandt.[25]

To show the effect of the pore size distribution on the overall concentration dependence of the partitioning, we plotted $K$ in dashed lines for $R_g/R_p = 0.2$, 0.4, 0.6, 0.8, and 1.0 in Figure 10. The solid line represents $K$ for $R_g/R_p = 1$ in the absence of the pore size distribution. The diffuse transition observed in the interferometry is better fitted by the curves calculated for the pore size distribution. Also note the diffuse nature in the weak-to-strong penetration transition on double linear scale.

(4) An overestimate in $K_0$ results in an increase in $K(w_{Et})$, and therefore moves a point in Figure 13 upward and to the right, away from the theoretial values.

(5) A polydispersity that exists in the polystyrene standards can diffuse the transition. Presence of low molecular weight components makes the osmotic pressure to increase more slowly as the concentration increases than in the perfectly monodisperse polymer solution.[35] This effect may, however, be counterbalanced by the preferred migration of low molecular weight components into the pore channels.

We consider that the pore size distribution is the largest factor in diffusing the weak-to-strong penetration transition, although it is not conclusive.

## Concluding Remarks

We applied Jamin interferometry and digital image analysis to measure the concentration of polymer in the pore channels of a porous medium in equilibrium with an external polymer solution in a wide concentration range. The transition from weak to strong penetration was observed for all the chain dimensions studied, but the transition was diffuse. Studies are in progress for the partitioning of polymer with a porous glass bead with a smaller pore size, and hence a stronger confinement. Also in progress is a development of interferometry to measure the concentration in porous silica beads of diameter about 0.05 mm packed in a bed. The equilibration time will be substantially smaller.

The interferometry can also be applied to measurements of surface adsorption with various surface functional groups on pore walls. Other extensions include a study of partitioning inversion that is predicted to

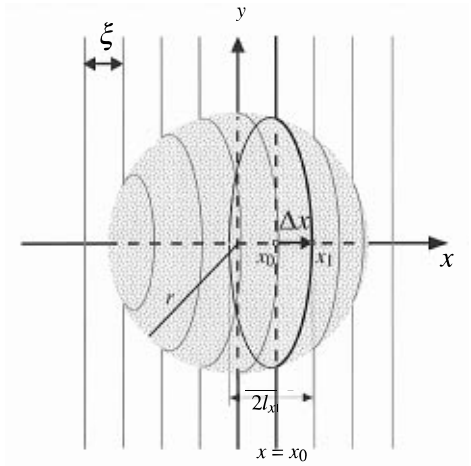


**Figure 14.** The fringe pattern in the image of a spherical medium follows an elliptic arc. See text for definitions of the symbols.

occur when a small amount of high molar mass fraction is added in the external solution.[36] Studies of concentration equilibrium of a ternary polymer solution may reveal the nature of the interaction between polymers in a common solvent.

**Acknowledgment.** I acknowledge Shell Development Co. for kindly supplying porous glass beads. I appreciate Anil Dube for valuable assistance.

## Appendix: Geometry of the Interference Pattern

This appendix explains the geometry of an interference pattern expected for a perfectly spherical, transparent bead suspended in a liquid. The difference $\delta n$ in the refractive index between the bead and the liquid is assumed to be small.

A coordinate system is introduced, for an image of the bead of radius $r$, with the origin at the center of the image and the $y$ axis parallel to the background fringe pattern with period $\xi$; see Figure 14. The photons that image at $(x, y)$ have traveled the thickness $t$ of the sphere given by $t = 2(r^2 - x^2 - y^2)^{1/2}$. A dark fringe is a trace of points that have the same difference in the optical path between the two beams. Outside of the bead image, or equivalently, in the background image where $\delta n = 0$, the contour of a dark fringe is given by $x = x_0$, where $x_0$ is the $x$-intercept of the fringe. The portion of the fringe within the bead image then follows the contour equation:

$$\frac{t\delta n}{\lambda} = \frac{x - x_0}{\xi} \tag{A1}$$

which is equivalent to

$$(x - x_0)^2 a^2 = r^2 - x^2 - y^2 \tag{A2}$$

where $a \equiv \lambda/(2\xi\delta n)$. We thus find that the contour is an ellipse centered at $(a^2x_0/(1+a^2), 0)$ and a semiminor axis $l_x \equiv \{[r^2 - a^2x_0^2/(1 + a^2)]/(1 + a^2)\}^{1/2}$ in the $x$ direction. On inspection of eq A2, we also find that the ellipse inscribes the circle $x^2 + y^2 = r^2$ (edge of the bead image) at $x = x_0$ and $y = \pm(r^2 - x_0^2)^{1/2}$ when $|x_0| < r$. The fringe within the circle is then an arc of the ellipse. When $|x_0| > r$, in contrast, the fringe is a closed ellipse enclosed in the circle, and the corresponding outside fringe runs off the bead image.

When the right-side arc represents the in-circle fringe, the arc intercepts the $x$ axis at $x_1 = a^2x_0/(1 + a^2) + l_x$. The displacement $\Delta x$ of the fringe at the equator is given by

$$\Delta x = x_1 - x_0 = (r^2 - x_1^2)^{1/2}/a \tag{A3}$$

Therefore, a plot of $\Delta x$ as a function of $x_1$ is on another elliptic arc. The displacement peaks at $x_1 = 0$, i.e., when the fringe passes through the center of the bead image. The maximum displacement is given by $\Delta x_m = r/a = 2r\xi\delta n/\lambda$, from which it follows that

$$\Delta x_m/\xi = d\delta n/\lambda \tag{A4}$$

where $d = 2r$. This equation was used to estimate $\delta n$ from the image analysis of the interference pattern.

As $\xi$ increases, the interference pattern changes, and most ellipses close, as seen in Figure 5. When $\xi$ is comparable to the bead diameter, the number of closed ellipses can also give an estimate of $\Delta x_m/\xi$. The condition for the elliptic arc that corresponds to the exterior fringe with contour $x = x_0 < -r$ to be closed is given as $r > |x_0|a/(1 + a^2)^{1/2}$. Thus, $-r(1+a^2)^{1/2}/a < x_0 < -r$ This condition guarantees that the two intercepts of the ellipse with the $x$ axis are in the interior of the bead image. Let $x_0 = -r - j\xi$; then $j$ must be in the range $0 < j < (r/\xi)\,[(1 + a^2)^{1/2}/a - 1]$. The number of closed ellipses that can be observed is equal to the largest integer that does not exceed $(r/\xi)[(1 + a^2)^{1/2}/a - 1]$. When we observe $m$ closed ellipses, we can tell that $m < (r/\xi)[(1 + a^2)^{1/2}/a - 1] < m + 1$. Therefore,

$$[m(m + d/\xi)]^{1/2} < d\delta n/\lambda < [(m + 1)(m + 1 + d/\xi)]^{1/2} \tag{A5}$$

For a given $d/\xi$, $d\delta n/\lambda = \Delta x_m/\xi$ needs to be in a window given above. The width of the window can be reduced by employing a larger period $\xi$. This criterion helps indexing when the image toward the edge of the bead is not clear.

## References and Notes

(1) Giddings, J. C. *Unified Separation Science*; John Wiley: New York, 1991.
(2) Casassa, E. F. *J. Polym. Sci., Polym. Lett. Ed.* **1967**, *5*, 773.
(3) Casassa, E. F.; Tagami, Y. *Macromolecules* **1969**, *2*, 14.
(4) de Gennes, P.-G. *Scaling Concepts in Polymer Physics*; Cornell University Press: Ithaca, NY, 1979.
(5) Giddings, J. C.; Kucera, E.; Russell, C. P.; Myers, M. N. *J. Phys. Chem.* **1968**, *72*, 4397.
(6) Gaylord, R. J.; Lohse, D. L. *J. Chem. Phys.* **1976**, *65*, 2779.
(7) Cifra, P.; Bleha, T.; Romanov, A. *Polymer* **1988**, *29*, 1664.
(8) Bleha, T.; Cifra, P.; Karasz, F. E. *Polymer* **1990**, *31*, 1321.
(9) Yethiraj, A.; Hall, C. K. *Mol. Phys.* **1991**, *73*, 503.
(10) Kierlik, E.; Rosinberg, M. L. *J. Chem. Phys.* **1994**, *100*, 1716.
(11) Priest, R. G. *J. Appl. Phys.* **1981**, *52*, 5930.
(12) Davidson, M. G.; Suter, U. W.; Deen, W. M. *Macromolecules* **1987**, *20*, 1141.
(13) Teraoka, I.; Langley, K. H.; Karasz, F. E. *Macromolecules* **1992**, *25*, 6106.
(14) Bleha, T.; Mlýnek, J.; Berek, D. *Polymer* **1980**, *21*, 798.
(15) Glandt, E. D. *AIChE J.* **1981**, *27*, 51.
(16) Anderson, J. L.; Brannon, J. H. *J. Polym. Sci., Polym. Phys. Ed.* **1981**, *19*, 405.
(17) Bleha, T.; Spychaj, T.; Vondra, R.; Berek, D. *J. Polym. Sci., Polym. Phys. Ed.* **1983**, *21*, 1903.
(18) Brannon, J. H.; Anderson, J. L. *J. Polym. Sci., Polym. Phys. Ed.* **1982**, *20*, 857.
(19) Cifra, P.; Bleha, T.; Romanov, A. *Makromol. Chem., Rapid Commun.* **1988**, *9*, 355.
(20) Satterfield, C. N.; Colton, C. K.; Turckheim, B. D.; Copeland, T. M. *AIChE J.* **1978**, *24*, 937.

(21) Daoud, M.; Cotton, J. P.; Farnoux, B.; Jannink, G.; Sarma, G.; Benoit, H.; Duplessix, R.; Picot, C.; de Gennes, P. G. *Macromolecules* **1975**, *8*, 804.
(22) Ohta, T.; Oono, Y. *Phys. Lett.* **1982**, *89A*, 460.
(23) Teraoka, I.; Langley, K. H.; Karasz, F. E. *Macromolecules* **1993**, *26*, 287.
(24) Daoud, M.; de Gennes, P. G. *J. Phys. (Paris)* **1977**, *38*, 85.
(25) Thompson, A. P.; Glandt, E. D., submitted to *Macromolecules*.
(26) Sernetz, M.; Bittner, H. R.; Baumhoer, C.; Schwarz, S.; Willems, H. *Stud. Surf. Sci. Catal.* **1987**, *39*, 461.
(27) Sernetz, M.; Bittner, H. R.; Willems, H.; Baumhoer, C. In *The Fractal Approach to Heterogeneous Chemistry*; Avnir, D., Ed.; John Wiley: New York, 1989.
(28) Huber, K.; Bantle, S.; Lutz, P.; Burchard, W. *Macromolecules* **1985**, *18*, 1461.
(29) Bishop, M. T.; Langley, K. H.; Karasz, F. E. *Macromolecules* **1989**, *22*, 1220.
(30) Dube, A.; Teraoka, I., in preparation.
(31) Zhou, Z.; Teraoka, I.; Langley, K. H.; Karasz, F. E. *Macromolecules* **1994**, *27*, 1759.
(32) Dube, A.; Teraoka, I. *Macromolecules* **1995**, *28*, 2592.
(33) Cotton, J. P. *J. Phys. (Paris)* **1980**, *41*, L-231.
(34) Noda, I.; Kato, N.; Kitano, T.; Nagasawa, M. *Macromolecules* **1981**, *14*, 668.
(35) des Cloizeaux, J.; Jannink, G. *Polymers in Solution: Their Modelling and Structure*; Clarendon Press: Oxford, 1990.
(36) Teraoka, I.; Zhou, Z.; Langley, K. H.; Karasz, F. E. *Macromolecules* **1993**, *26*, 3223.

MA951146Z